JACS
JOURNAL OF THE AMERICAN CHEMICAL SOCIETY
Article
pubs.acs.org/JACS

The Polyphenol EGCG Inhibits Amyloid Formation Less Efficiently at Phospholipid Interfaces than in Bulk Solution

Maarten F. M. Engel,[†] Corianne C. vandenAkker,[†] Michael Schleeger,[†,‡] Krassimir P. Velikov,[§,∥] Gijsje H. Koenderink,[†] and Mischa Bonn*[,†,‡]

[†]FOM Institute AMOLF, Science Park 104, 1098 XG, Amsterdam, The Netherlands

[‡]Department of Molecular Spectroscopy, Max Planck Institute for Polymer Research, Ackermannweg 10, 55128 Mainz, Germany

[§]Unilever R&D Vlaardingen, Olivier van Noortlaan 120, 3133 AT Vlaardingen, The Netherlands

[∥]Soft Condensed Matter, Debye Institute for Nanomaterials Science, Department of Physics and Astronomy, Utrecht University, Princetonplein 5, 3584 CC, Utrecht, The Netherlands

Supporting Information

ABSTRACT: Age-related diseases, like Alzheimer's disease and type 2 diabetes mellitus, are characterized by protein misfolding and the subsequent pathological deposition of fibrillized protein, also called amyloid. Several classes of amyloid-inhibitors have recently been tested, traditionally under bulk conditions. However, it has become apparent that amyloid fibrils and oligomers assemble and exert their cytotoxic effect at cellular membranes, rather than in bulk solution. Knowledge is therefore required of inhibitor activity specifically at the phospholipid membrane interface. Here we show, using surface-specific sum-frequency generation (SFG) spectroscopy and atomic force microscopy (AFM), that the commonly used (−)-epigallocatechin gallate (EGCG) is a much less efficient amyloid inhibitor at a phospholipid interface than in bulk solution. Moreover, EGCG is not able to disaggregate existing amyloid fibrils at a phospholipid interface, in contrast to its behavior in bulk. Our results show that interfaces significantly affect the efficiency of inhibition by EGCG inhibitors and should therefore be considered during the design and testing of amyloid inhibitors.

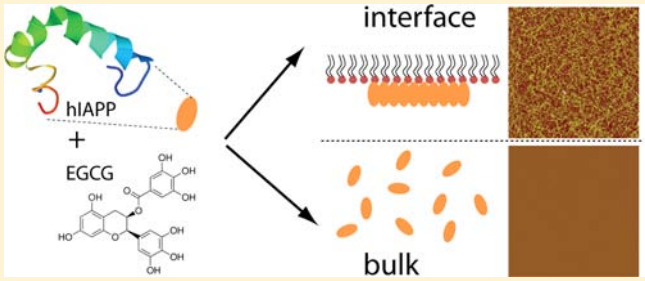

INTRODUCTION

Many protein misfolding diseases, such as Alzheimer's disease and type 2 diabetes mellitus, are characterized by the pathological deposition of amyloid fibrils.[1−3] Current hypotheses suggest that these fibrils, and/or their oligomeric precursors, cause cell death by disrupting cellular membranes.[4−6] Consequently, the inhibition of the formation of fibrils or oligomers has been a focus in the development of drugs for misfolding diseases.[7,8] In recent years several types of inhibitors have been tested for their ability to reduce amyloid cytotoxicity, using either cells[9−12] or in vitro model systems.[13−17] An important class of inhibitors is made up of polyphenols, which are thought to interact with amyloidogenic proteins via aromatic $\pi-\pi$ interactions,[13,14,18−20] though the precise mechanism is an issue still under debate.[21,22] A particularly promising inhibitor is (−)-epigallocatechin gallate (EGCG), a natural component of green tea. This polyphenol inhibits fibrillation of several amyloidogenic peptides[9,20,23−25] and has even been shown to disaggregate existing fibrils.[22,23,26,27] Further, EGCG protects cells against amyloid-induced toxicity.[9,22,23] During *in vitro* studies, inhibitors are typically tested under bulk conditions, for which aggregating peptide and inhibitor are diffusing freely in solution, as has also been the case for studies on EGCG.[9,22−27] However, it is the cellular membrane, and not bulk solution, where amyloid fibrils and oligomers are thought to assemble and exert their cytotoxic effect.[4−6] In recent experiments on lipid- or glycosaminoglycan-mediated amyloid formation, modifications of inhibitor effectivity could be demonstrated.[28−31] It is therefore vital to know whether inhibitors are also effective at the phospholipid membrane interface.

Many techniques have become available for measuring fibril formation and its inhibition in bulk solution, such as the thioflavin T (ThT) assay and electron microscopy.[32] However, here we want to study these processes specifically and exclusively at the phospholipid interface. We exploit the unique sensitivity and spatial selectivity of vibrational sum-frequency generation (VSFG) to study amyloid fibrillation at the phospholipid interface. This approach was recently pioneered by the Yan group.[33,34] Here we use this technique to elucidate the effect of EGCG on fibril formation. In addition, atomic force microscopy (AFM) in combination with the Langmuir−Blodgett technique, to selectively probe only interfacial

Received: April 2, 2012
Published: August 13, 2012

   dx.doi.org/10.1021/ja3031664 | J. Am. Chem. Soc. 2012, 134, 14781−14788

molecules, is used to investigate the morphology of species produced during aggregation at the phospholipid interface.

VSFG provides information about the conformation and orientation of molecules at interfaces.[34−36] In VSFG, two pulsed laser beams, one at visible and one at infrared (IR) frequency, are focused to overlap at the interface. As a result of the interaction of the laser fields with molecules at the surface—and only those at the surface—light at the sum frequency of the visible and IR beams may be generated. When the IR frequency matches that of a surface vibrational mode, this process may be resonantly enhanced. Protein conformations can be investigated through the C═O vibrations of the protein backbone (amide I region, 1600−1700 cm^{-1}), where the characteristic β-sheet structure of amyloid fibrils can be distinguished from structures such as random coil and α-helix.[37] VSFG spectroscopy is a sensitive, label-free method that so far has seen limited application in the study of interfacial amyloid secondary structure.[33,34,38]

Human islet amyloid polypeptide (hIAPP) forms fibrillar amyloid deposits in the pancreatic islets of Langerhans of patients with type 2 diabetes mellitus.[2] hIAPP fibrils and/or oligomers are thought to be involved in the death of the insulin-producing cells in these islets.[2−4,6] Like many amyloidogenic peptides, nonaggregated hIAPP is mainly unstructured, while fibrillar hIAPP is rich in β-sheet structure.[39] Current models of membrane-mediated IAPP fibrillation are based on transiently populated α-helical intermediates.[40,41] It is thought that binding of these species to the membrane surface, especially the attachment of cationic amino acid residues to anionic membranes, facilitates an increase in the local protein concentration. Thereby conformational switching from helical to β-sheet structures and subsequent fibril growth is mediated. Different mechanisms of how amyloids induce cytotoxicity have been proposed,[42,43] such as the disruption of membranes by pore formation or nonspecific interaction.[44] We have chosen hIAPP for two reasons: First, the details of the aggregation of hIAPP, both in bulk and at the interface, have been described extensively.[3,39,45−48] Second, a recent study has shown that EGCG efficiently inhibits hIAPP aggregation in bulk.[23] As a model membrane, we use monolayers of the negatively charged lipid 1,2-dihexadecanoyl-*sn*-glycero-3-phospho-(1′-*rac*-glycerol) (DPPG), since IAPP−lipid interactions have been investigated extensively with this system.[33,47,49] Also, DPPG accelerates IAPP aggregation, which allows for reasonable VSFG measuring times.[33]

Here we combine VSFG with AFM to investigate IAPP aggregation and its inhibition by EGCG exclusively at a phospholipid interface. We demonstrate that EGCG has a strongly reduced efficiency to inhibit the formation of hIAPP amyloid fibrils at the phospholipid interface, in contrast to its behavior in bulk. Moreover, we show that while EGCG disaggregates hIAPP fibrils in bulk, EGCG has no effect on fibrils at the phospholipid interface, even when present in large molar excess.

EXPERIMENTAL SECTION

Preparation of Solutions and Monolayers. Synthetic hIAPP (Bachem H-7905) stock solutions were prepared by dissolving freeze-dried peptide powder in Milli-Q water to a final concentration of ∼1 mg/mL. This solution was filtered using a 0.2 μm filter. Immediately afterward, the concentration of hIAPP was measured using the absorbance at 280 nm and the known extinction coefficient of 1280 cm^{-1} M^{-1}.[50] The final concentration of the stock solution was typically between 120 and 160 μM. The solution was aliquoted and immediately stored at −80 °C until use. Once thawed, the contents of the tube were used within minutes, and left-over solution was discarded. EGCG (>95%, Sigma-Aldrich E4143) stock solutions were freshly prepared before each experiment as a 1 mM solution in Milli-Q water. All experiments were performed using a 10 mM sodium phosphate buffer at pH 7.4 which was filtered using a 0.2 μm filter before each experiment. The monolayer was prepared in a circular Teflon trough with a diameter of 80 mm. First, the trough was filled with 25 mL buffer either with or without 1 μM EGCG. Next, hIAPP stock solution was added to obtain a final hIAPP concentration of 1 μM. The solution was carefully mixed by pipetting up and down using a 1 mL pipet. After incubation for 10−15 min, 16 drops (0.5 μL) of a 1 mM solution of DPPG (Avanti Polar Lipids) in chloroform were evenly spread on the surface to obtain 107 $Å^2$ per phospholipid molecule (defined in absence of peptide).

These conditions were chosen in accordance with recent experiments of Fu et al.[33] The resulting surface pressure is around 30 mN/m, corresponding to the packing density of lipids in biological membranes.[51] The phospholipid−hIAPP interface was heterogeneous, i.e., SFG spectra were different at different locations at the interface likely due to clustering of fibrils [see Figure S5, Supporting Information (SI)]. To average the signal over a large surface area, the trough was rotated at ∼10 rpm.

VSFG Spectroscopy. The VSFG spectroscopy setup has been described in detail elsewhere.[52] Briefly, a visible beam (vis) (800 nm, 20−30 μJ/pulse, spectral bandwidth of 25 cm^{-1}) is overlapped at the sample position with an infrared (IR) beam (2−3 μJ/pulse, 150 fs broadband), which is centered at 1675 cm^{-1} and has a spectral bandwidth of 150 cm^{-1}. Both beams are focused down to ∼100 μm beam waist. The incident angles of the vis and IR beams are 35° and 40°, respectively, both defined relative to the surface normal. The SFG light generated by the sample is detected with a monochromator connected to a charge-coupled device camera. All spectra were collected at 23.0 ± 0.2 °C under unpolarized SFG, s-polarized vis, and p-polarized IR conditions and integrated over 6 min. In contrast to recently published VSFG data on hIAPP aggregation,[33] we observe no amide I signal for hIAPP fibrillation using psp polarization conditions (corresponding to p-polarized SFG, s-polarized vis, and p-polarized IR settings).[38] To not unnecessarily lose signal photons, we decided to omit the output polarizer. Spectral analysis included background subtraction and division by the reference signal from a z-cut quartz plate that was taken immediately before or after the spectrum of the monolayer. Spectral fitting was performed using a three-component (two for the amide I signal and one for the phospholipid signal) Lorentzian model and included the maximum entropy method (MEM) analysis to verify the fit.[35] The equation used for the fit has been described previously and is commonly used to fit VSFG spectra.[33,35,37] The fitting procedure yields values for the amplitude and phase of the nonresonant susceptibility and for the amplitude, wavenumber, and line width (full width at half-maximum, fwhm) of each component, as shown in Tables S1 and S2. Fitting was performed in Igor Pro 6.2 (WaveMetrics, Inc.) using a global fit procedure for all spectra from a single aggregation experiment, with the nonresonant contribution, the wavenumber, the full width at half height, and the peak maximum position linked for all spectra during the fit. The relative contribution of each component in the amide region was calculated by dividing the amplitude by the fwhm, followed by normalization to the maximum of the amide signal intensity. For the 1672 cm^{-1} component, this value is named "SFG β-sheet/turn", as plotted in Figures 2a and 3b. The value obtained is proportional to the amount of secondary structure when assuming that the IR and Raman dipole do not depend on the secondary structure and that orientation effects are canceled out by the random orientation of the fibrils in the plane of the surface. The error is estimated to be ±0.07 (au) for all SFG data points in Figures 2a and 3b, based on the variation in fit results when different fit assumptions are made (for example, with or without requiring the widths of the resonances to be identical for all fits).

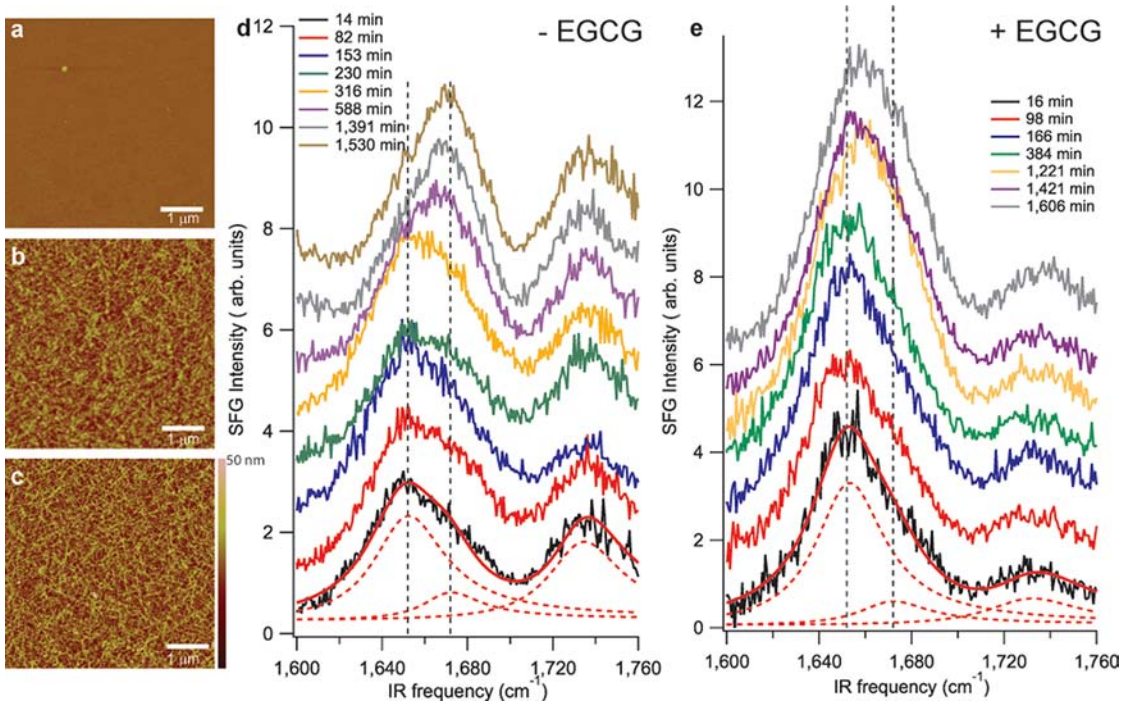

Figure 1. AFM images and SFG spectra measured during hIAPP aggregation at the phospholipid interface in the presence or absence of EGCG. AFM images after hIAPP aggregation for (a) 10 and (b) 1020 min in the absence of EGCG, and (d) VSFG spectra taken at various time points. (c) AFM image after hIAPP aggregation in the presence of EGCG at a 1:1 hIAPP:EGCG molar ratio for 1020 min, and (e) corresponding VSFG spectra. The vertical dashed lines in panels d and e indicate IR frequencies of 1652 and 1672 cm^{-1}, respectively. Red lines through the bottom spectra are exemplary results of the global fit; the dashed red lines show the three individual components of each fit.

Atomic Force Microscopy (AFM). Samples for AFM were prepared using the Langmuir−Blodgett technique and a MicroTrough X (Kibron). The trough area was filled with 55 mL buffer, with or without 1 μM EGCG, and the surface area was set to 110 cm^2 using movable barriers to obtain the same area to volume ratio as in the trough used for SFG measurements. A freshly cleaved piece of mica (15 × 15 mm) was submerged, and hIAPP was added to obtain a final concentration of 1 μM. The solution was carefully mixed by pipetting up and down using a 1 mL pipet. After a stable surface pressure of ∼20 mN/m was reached, 32 drops (0.5 μL) of a 1 mM solution of DPPG in chloroform were evenly spread over the surface to obtain 107 $Å^2$ per lipid (defined in absence of peptide) after which the surface pressure increased to 30 mN/m. Next, the mica was pulled up through the surface at 5 mm/min while maintaining a constant surface pressure of 30 mN/m. The mica was air dried and used for AFM analysis using tapping mode AFM in air (Dimension 3100 scanning probe microscope, Veeco). Silicon cantilevers with a force constant of 5 N/m were used. Images were flattened using Nanoscope 6.14 software. For analysis of samples from the ThT test (see below), 40 μL samples were taken from the wells of the mitrotiter plates (see below) and incubated for 5 min on freshly cleaved mica, washed 2 to 3 times with 1 mL of Milli-Q water, and air dried. For the AFM analysis of the ThT experiment, a concentration of 10 μM hIAPP was used since 1 μM was too low for AFM analysis of bulk aggregation. The ThT curves for 10 μM also show complete inhibition of fibril formation in the presence of EGCG.

ThT Kinetics. The kinetics of hIAPP fibril formation was measured using the fluorescence intensity increase upon binding of the fluorescent dye ThT to hIAPP fibrils, a commonly used method to detect amyloid fibrils.[53] A plate reader (PerkinElmer Victor X3) was used to perform ThT experiments in standard 96-well flat-bottom black microtiter plates (Nunc 237105) in combination with a 430 nm excitation filter and a 480 nm emission filter. The assay was started by adding a few μL of a 140 μM hIAPP stock solution in Milli-Q to a solution of 10 μM ThT in 10 mM sodium phosphate at pH 7.4. The final hIAPP concentration was either 1 or 10 μM, and the total volume in each well was 150 μL. When required, EGCG (at a final concentration of 1 or 10 μM, always at a 1:1 molar ratio of hIAPP:EGCG) was added before the addition of hIAPP. The microtiter plate was covered using a transparent self-adhesive film to prevent evaporation from the wells. The microtiter plate was shaken before the measurement for 10 s by using the shaking function of the plate reader. Fluorescence was measured from the top every 5 min at 23 ± 1 °C.

Fourier Transform Infrared Spectroscopy (FT-IR). Infrared transmission measurements were carried out on a Vertex 70 FT-IR spectrometer (Bruker Optics, Ettlingen, Germany) using a deuterated triglycine sulfate detector (DTGS). The spectral resolution was 4 cm^{-1}, and for each measurement 256 spectra were averaged. The Blackmann−Harris 3-term apodization function was used for the Fourier transformation. Bulk fibrils of hIAPP were grown in a 10 μM solution for 18 h while agitated. The sample was concentrated by ultrafiltration using centrifugal filters with molecular weight cutoff of 10 kDa (Amicon Ultra-4, Millipore, Cork, Ireland). The aqueous buffer was exchanged by a deuterium oxide-based sodium phosphate buffer at pD 7.4 by 10-fold dilution and concentration for 3 times. The sample of the approximate concentration of 200 μM was incubated for 5 h to allow for a full H/D exchange. The fibril suspension was mixed with an EGCG solution in deuterium oxide to yield a 1:1 molar ratio. The FT-IR transmission cuvette based on two CaF_2 windows was immediately assembled under a stream of nitrogen and sealed with vacuum grease (Baysilone-Paste, Bayer, Leverkusen, Germany). Spectral recording was started 20 min after mixing of the fibrils with ECGC, due to the assembling of the cuvette and the depletion time of atmospheric water vapor in the spectrometer. Spectra were recorded every 5 min for 12 h. No baseline correction was performed; the second derivative spectra were calculated using the OPUS software. Attenuated total reflection (ATR) spectra were measured on a single reflection ATR cell equipped with a diamond crystal (Spectra-Tech Foundation Performer, Thermo Scientific, Waltham, MA) on a Nicolet 730 FT-IR spectrometer (Thermo Scientific). Five μL of the aqueous

dx.doi.org/10.1021/ja3031664 | J. Am. Chem. Soc. 2012, 134, 14781−14788

hIAPP sample was deposited on the ATR crystal by drying at room temperature.

RESULTS

We used VSFG and AFM to gain insight into the inhibition of amyloid fibril formation by EGCG specifically at the physiologically relevant phospholipid interface. The phospholipid interface was obtained by depositing phospholipid molecules at the air−water interface of a buffered solution of hIAPP molecules in a trough. First, we examined assembly of hIAPP into amyloid fibrils at the phospholipid interface in the absence of EGCG. Addition of nonaggregated hIAPP to buffer, to a final peptide concentration of 1 μM, resulted in an increase of the surface pressure to ∼20 mN/m, showing that nonaggregated hIAPP is surface active, like many amphiphilic peptides. This observation is in agreement with earlier studies of hIAPP[46] and other amyloidogenic proteins and peptides.[54,55] Subsequently, the negatively charged phospholipid DPPG was deposited at the interface up to a surface pressure of ∼30 mN/m, which corresponds to the packing density of lipids in biological membranes.[51] At this surface pressure, a DPPG monolayer adopts, at room temperature, the liquid condensed phase.[56] In the absence of lipids, hIAPP does not convert to β-sheet-rich structures on the time scale of our VSFG experiments (see Figure S1 and Table S3). We exclude the presence of pre-existing aggregates by the fact that we observe a characteristic lag phase in ThT fluorescence assays. Presence of pre-existing aggregates would have resulted in an immediate increase in fluorescence intensity.[1] Additionally, no amyloid fibrils are observed by AFM 10 min after adding lipids to the freshly prepared hIAPP solution (Figure 1a). However, after 17 h of incubation, the interface showed the abundant presence of fibrils with diameters in the range of 3−7 nm, typical of amyloid fibrils (Figure 1b).

VSFG enabled us to follow the kinetics of fibrillation specifically at the phospholipid interface, as shown in Figure 1d. The peptide and the phospholipid both contribute to the spectra but in different wavenumber regions. The phospholipid displays a carbonyl stretch vibration around 1730 cm^{-1}, while the peptide shows peaks in the amide I region (1600−1700 cm^{-1}). Note that EGCG has no vibrational modes in this frequency region. We have fitted a three-component Lorentzian function to the SFG spectra using one component for the carbonyl stretch vibration of DPPG (1730 cm^{-1}) and two components to describe the amide I region (see SI methods and a list of fit parameters in Tables S1 and S2; an example fit to the spectrum after 14 min is shown as a red line in Figure 1d). The two amide I components are centered at 1652 and 1672 cm^{-1}, suggesting a contribution of α-helix or random structure and β-sheet or turns, respectively.[33,34,36,57,58] At early times, the amide I region is dominated by α-helix or random structure (1652 cm^{-1}), between which we cannot distinguish. These spectra are consistent with the AFM images showing that the peptide is initially nonaggregated. However, as time progresses, the contribution of β-sheet/turns (1672 cm^{-1}) increases. After 8−10 h, the peptide is fully converted from α-helix or random structure to β-sheet or turns, consistent with prior SFG measurements.[33,34] As amyloid fibrils are characterized by the dominant presence of β-sheet content, we assign the increase in the 1672 cm^{-1} component mainly to increased β-sheet structure, rather than β-turns.[33,34,36,57,58] We assume, that the β-sheet content is directly related to formation of mature fibrils. In the absence of lipids, hIAPP does not convert to β-sheet-rich structures at the surface on the time scale of our SFG experiment (see Figure S1 and Table S3). This confirms the catalyzing role of lipids in hIAPP aggregation, observed previously for liposomes.[49]

To assess the influence of EGCG on fibrillation both in bulk solution and at the phospholipid interface, we followed hIAPP fibrillation in both situations in the presence of an equimolar amount (1 μM) of EGCG. For the quantification of bulk fibril formation, we use a ThT assay, in which the thioflavin fluorescence serves as a reporter for the presence of fibrils (Figure 2a).[53] Note that the ThT assay cannot separate

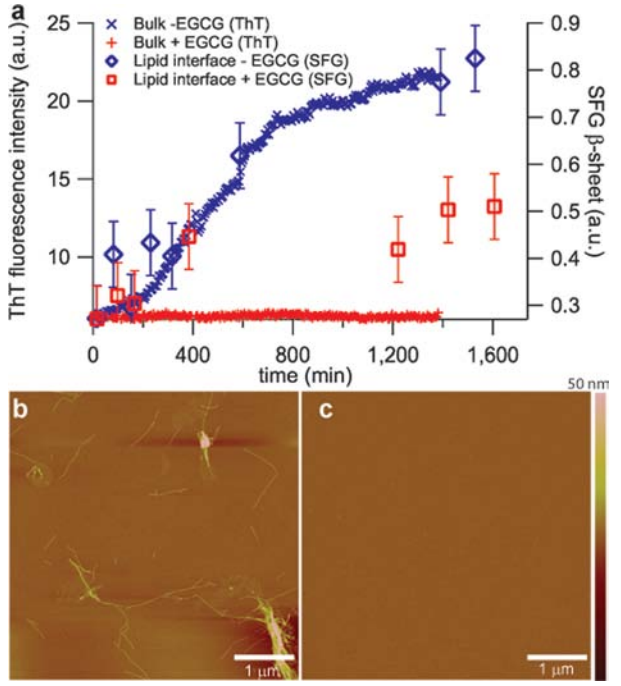

Figure 2. Comparison of the inhibitory effect of EGCG on hIAPP fibrillation in bulk and at the phospholipid interface. (a) The formation of hIAPP amyloid fibrils in bulk was measured using a ThT fluorescence assay, showing the characteristic sigmoidal increase in fibril yield in the absence of EGCG (×) and virtually complete inhibition of fibril growth in the presence of EGCG at a 1:1 molar ratio (+). The formation of amyloid fibrils at the phospholipid interface was measured by determining the relative β-sheet intensity from the VSFG spectra, in absence (◇) and presence (□) of EGCG. AFM confirms that (b) hIAPP fibrils have grown in bulk solution in the absence of EGCG and that (c) an equimolar amount of EGCG completely inhibits fibril formation. From the SFG results, it is apparent that the inhibition efficiency of EGCG is much reduced at the lipid interface.

interfacial and bulk contributions to the fluorescence; its application is therefore restricted to bulk experiments. In agreement with previous reports in bulk,[23] 1 μM of EGCG suffices to completely inhibit hIAPP aggregation in bulk experiments; the thioflavin fluorescence is completely suppressed in the presence of EGCG. AFM images confirm that no fibrils are formed under bulk conditions when EGCG is present at an equimolar concentration (Figure 2c), whereas abundant fibrils are present in absence of EGCG (Figure 2b). In contrast, the EGCG inhibitory activity is much reduced at the phospholipid interface; AFM images of the interface transferred onto mica showed the abundant presence of fibrils (Figure 1c), despite the presence of EGCG. Consecutive VSFG spectra taken during 24 h incubation of hIAPP in the presence of

dx.doi.org/10.1021/ja3031664 | J. Am. Chem. Soc. 2012, 134, 14781−14788

EGCG confirmed that there was significant conversion of hIAPP secondary structure from α-helix or random structure (1652 cm^{-1}) to β-sheet (1672 cm^{-1}) (see Figure 1e). However, the shift in peak position of the entire amide I band, which is a convenient indicator of peptide aggregation,[33] is significantly less in the presence of EGCG (7 cm^{-1}) than in its absence (20 cm^{-1}). Note that the relative SFG intensities of the phospholipid and hIAPP contributions in spectra taken in the presence of EGCG (~0.8 and 5 au, respectively) are different than in the spectra taken in its absence (~1 and 3 au, respectively), due to slightly smaller amounts of lipids that were deposited on the subphases for the experiment with EGCG. Fewer lipids result in a lower signal at 1730 cm^{-1} and leave more room at the surface for fibrils, causing a larger intensity in the 1652 cm^{-1} region. These small differences in surface lipids do not affect the interfacial fibrillation kinetics. To obtain quantitative information about the inhibition of hIAPP fibrillation at the phospholipid interface by EGCG, we fitted the contributions of the α-helix/random structure (1652 cm^{-1}) component and the β-sheet (1672 cm^{-1}) component during hIAPP aggregation. Both contributions are expressed as the amplitude of the contribution to interfacial vibrational response divided by the full width at half-height (see methods and Tables S1 and S2). The resulting values are normalized so that at every time the total amide I contribution equals one. As shown in Figure 2a, the relative amount of β-sheet intensity increases with time, both in the presence and absence of EGCG. However, in the presence of EGCG, the spectral amplitude reflecting the formation of β-sheet structure is reduced by a factor of 2. This suggests that, while it shows some activity also at the phospholipid interface, EGCG is markedly less effective at the interface than in bulk, where the inhibition is close to 100% in the same time (Figure 2a).

Another characteristic of EGCG that has been demonstrated under bulk conditions is its ability to disaggregate existing fibrils into unstructured smaller species.[9,23,26,27] We indeed observe this effect in our ThT assays when adding EGCG to preformed hIAPP fibrils in bulk conditions (Figure 3a), and we confirmed the breakdown of fibrils by AFM. Next, we asked whether EGCG is also able to reduce the β-sheet content of existing hIAPP fibrils at the phospholipid interface. We formed hIAPP fibrils at the phospholipid interface by incubation for 17 h in absence of EGCG and then recorded VSFG spectra during the incubation of EGCG with the pre-existing fibrils. These measurements showed that the β-sheet content of hIAPP fibrils at the interface, at a bulk hIAPP concentration of 1 μM, is not reduced by 1 μM EGCG, even after incubation for 2 days, in strong contrast with the situation in bulk (Figure 3a). Moreover, even at EGCG to hIAPP molar ratios of up to 1000, no disaggregation of interfacial hIAPP fibrils was observed, even after 24 h of incubation (Figure 3b). AFM measurements confirm that hIAPP fibrils indeed remain at the lipid interface (inset Figure 3b).

To test whether a structurally different type of fibrils is formed at the interface which is more resistant to EGCG than fibrils formed in bulk solution, we investigated the effect of EGCG on interfacial fibrils in the absence of lipids. Fibrils were collected after overnight incubation at the lipid interface. AFM imaging showed that preformed interfacial fibrils are disaggregated upon incubation with EGCG in bulk (Figure S6), which strongly suggests that the apparent resistance of IAPP amyloids against EGCG at the lipid monolayer interface is not

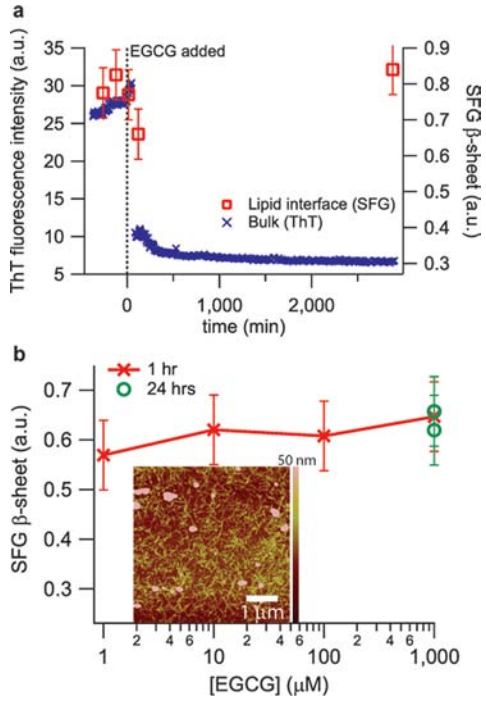

Figure 3. Effect of EGCG on preformed hIAPP fibrils in bulk and at the surface. (a) Kinetics of disaggregation of preformed hIAPP fibrils with EGCG at a 1:1 molar ratio in bulk, followed by a ThT assay (×), compared to disaggregation at a lipid interface, followed by SFG (□). The dotted line at $t = 0$ indicates the time of addition of EGCG to the fibrils. (b) The relative β-sheet/turn intensity from the VSFG spectra for incubation of preformed hIAPP fibrils for 1 h at the phospholipid interface (×) as function of EGCG concentration. Incubations for 24 h at 1 mM EGCG are also shown (○). The inset shows an AFM image of abundant hIAPP fibrils that remain at the DPPG interface after incubation with 100 μM EGCG for 24 h. The SFG spectra and fit parameters of the data in this figure are shown in Figure S2 and Tables S4 and S5.

an intrinsic (e.g., structural) property of the interfacial amyloid fibril itself.

In the analysis of the VSFG data we assume a direct correlation between β-sheet content of hIAPP and the formation of mature fibrils. From VSFG data, we cannot exclude, however, the presence of oligomeric forms of hIAPP containing β-sheet structure elements. Such oligomers might form as intermediates during fibrillogenesis or upon disaggregation by EGCG. To confirm that the β-sheet content is indeed an unambiguous marker of the fibril state of hIAPP, FT-IR experiments were performed. Changes in the secondary structure of hIAPP fibrils grown in bulk solution upon addition of ECGC were investigated by changes in the amide I absorption band. EGCG does not exhibit any FT-IR absorption band centered between 1680 and 1615 cm^{-1} (data not shown). Figure 4 shows the second derivative of the FT-IR absorption spectra (cf. Figure S7 for the raw absorption spectra). The air-dried hIAPP film yields a pronounced amide I band. The minima in the respective second derivative spectrum identify the various distinct contributions to the amide I band related to different secondary structure types (Figure 4a). The predominant β-sheet character of the dry amyloid sample is evident by a pronounced minimum at 1625 and a weaker one at 1673 cm^{-1}. Their spectral positions appear at remarkable low wavenumbers, indicating the strong hydrogen-bond interactions typical for amyloids. The latter minimum coincides with

dx.doi.org/10.1021/ja3031664 | J. Am. Chem. Soc. 2012, 134, 14781−14788

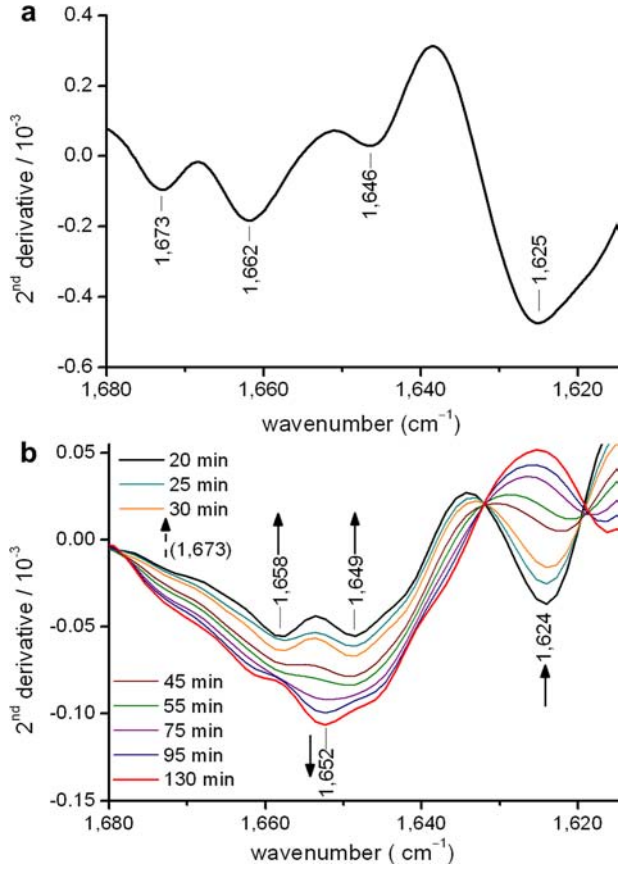

Figure 4. Second derivatives of the FT-IR absorption spectra in the spectral region of the amide I vibrational band of (a) the ATR-spectrum of the dry IAPP fibril film and (b) the transmission spectra of the IAPP disaggregation kinetics upon EGCG addition. The minima identify the center of the absorption bands, contributing to the respective FT-IR absorption spectrum. Bands at 1625 and 1673 cm^{-1} reveal the low- and high-frequency contribution of β-sheet secondary structure, present in the ATR spectrum and in the early kinetic spectra.

the β-sheet marker band present in the VSFG spectra (Figure 1d,e). The position of two additional minima at 1646 and 1662 cm^{-1} may originate from smaller contributions of helical and/or unordered structures in hIAPP fibrils.[59] Structural transitions during the dissolution process of a 1:1 molar mixture of hIAPP fibrils and EGCG are followed by transmission FT-IR. The sample was suspended in deuterium oxide buffer to separate the amide I vibration from the water bending vibrational mode. Whereas the FT-IR absorption bands in the unaltered absorption spectra were low in intensity and the amide I band was affected by the broad background contribution of deuterium oxide centered at 1555 cm^{-1} (cf. Figure S7b), the second derivative spectra clearly identify the different contributions to the amide I spectra (Figure 4b). The first spectrum, taken 20 min after mixing EGCG and hIAPP fibrils, strongly resembles the second derivative spectrum of the dry hIAPP fibrils (Figure 4a), indicating the predominant amyloid state of the sample. Slight shifts of the position of the minima can be attributed to the H/D exchange and the ongoing disaggregation process. The time dependence of disaggregation is demonstrated by the second derivative spectra measured at selected time points after mixing the hIAPP fibrils with EGCG as indicated in the legend of Figure 4b. All minima corresponding to the fibril state of hIAPP disappear successively within 130 min, most notably, including the minima corresponding to the β-sheet content of the sample. Simultaneously a new minimum is formed at 1652 cm^{-1}, which can be attributed to the formation of an α-helix.[59] The high α-helical content of the disaggregation products suggests that monomeric hIAPP is formed.[60] These results clearly demonstrate that a break-up of fibrillar structures would be apparent from the SFG spectra. The fact that the SFG intensity associated with β-sheet content remains after addition of EGCG thus demonstrates the inability of ECGC to disrupt fibrils at the lipid interface.

DISCUSSION

By using VSFG supported by FT-IR in combination with AFM, we were able to show that EGCG has a considerably lower capacity toward the inhibition of hIAPP fibril formation at a phospholipid interface and is unable to disrupt the β-sheet structure of existing fibrils, in strong contrast with the efficient inhibition of fibril formation and disruption of pre-existing fibrils in bulk. The phospholipid monolayer apparently stabilizes the fibrils toward EGCG. This stabilization is the result of noncovalent interactions at the interface, enabled by the amphiphilicity of both fibrils and lipids. The interaction between lipids and fibrils at the surface is also apparent from the contribution to the surface tension of both entities.

The molecular origin of the low fibril-inhibition efficiency of EGCG at the interface likely originates from the simple inability of EGCG to access the binding site on the peptide due to the peptide's presence at the interface. EGCG has been suggested to interact with amyloidogenic peptides and proteins via aromatic residues.[14,15,20] These hydrophobic aromatic residues will be contained within the hydrophobic part of the phospholipid−air interface, rather than pointing toward bulk water. EGCG is simply not present in the interfacial hydrophobic region as is evident from: (i) the absence of an increase of the surface pressure when EGCG is added under an air−water or an air−DPPG interface (see Figure S3) and (ii) the absence of SFG signal in the CH stretch spectral region (2800−3200 cm^{-1}) from an EGCG solution interface (see Figure S4). A role may also be played by the competitive interaction of EGCG with lipids, which would serve to further reduce its effective interfacial concentration. Indeed, EGCG has been reported to interact with the neutral phospholipid dipalmitoylphosphatidylcholine (DPPC) and to a lesser extent with negatively charged lipids.[61,62] Hence the low interfacial fibril disaggregation efficiency of EGCG is concluded to result from a negligibly low interfacial concentration of EGCG. This effect cannot even be negated by increasing the bulk concentration by several orders of magnitude (Figure 3b).

Disaggregation experiments of interfacial fibrils in the absence of lipids demonstrate that their resistance against EGCG is not a property of the fibrils itself, as it would be the case if fibrils formed at the lipid interface are different from fibrils in bulk solution (Figure S6). This observation is consistent with the hypothesis that the ECGC is simply not interacting with the fibrils at the lipid interface.

The combined results presented here demonstrate that EGCG only partially inhibits the formation of β-sheet structure at the phospholipid interface, being ~50% less efficient at the interface compared to bulk. Moreover, EGCG is not able to disaggregate existing fibrils at an interface during the course of our experiments; the phospholipid interface negatively affects the efficiency of the inhibitor. Given that current hypotheses

dx.doi.org/10.1021/ja3031664 | J. Am. Chem. Soc. 2012, 134, 14781−14788

suggest that it is the cellular membrane where amyloid fibrils and oligomers assemble and exert their cytotoxic effect, phospholipid interfaces should be considered during the design and *in vitro* testing of amyloid inhibitors. We show here that SFG spectroscopy in conjunction with AFM provides a useful assay for testing the activity of amyloid inhibitors specifically at interfaces.

■ ASSOCIATED CONTENT

Supporting Information

VSFG spectra together with the respective fit parameters of the spectra, AFM images of interfacial fibrils in the absence of lipids, and the FT-IR absorption spectra corresponding to the presented second derivative spectra. This material is available free of charge via the Internet at http://pubs.acs.org.

■ AUTHOR INFORMATION

Corresponding Author

bonn@mpip-mainz.mpg.de

Notes

The authors declare no competing financial interest.

■ ACKNOWLEDGMENTS

This work is part of the Industrial Partnership Programme (IPP) Bio(-Related) Materials (BRM) of the Stichting voor Fundamenteel Onderzoek der Materie (FOM), which is financially supported by the Nederlandse Organisatie voor Wetenschappelijk Onderzoek (NWO). The IPP BRM is cofinanced by the Top Institute Food and Nutrition and the Dutch Polymer Institute. This work is further supported by NanoNextNL, a micro- and nanotechnology consortium of the Government of The Netherlands and 130 partners.

■ REFERENCES

(1) Chiti, F.; Dobson, C. M. *Annu. Rev. Biochem.* **2006**, *75*, 333.
(2) Höppener, J. W. M.; Ahrén, B.; Lips, C. J. M. *N. Engl. J. Med.* **2000**, *343*, 411.
(3) Engel, M. F. M. *Chem. Phys. Lipids* **2009**, *160*, 1.
(4) Kayed, R.; Head, E.; Thompson, J. L.; McIntire, T. M.; Milton, S. C.; Cotman, C. W.; Glabe, C. G. *Science* **2003**, *300*, 486.
(5) Lashuel, H. A.; Lansbury, P. T. *Q. Rev. Biophys.* **2006**, *39*, 167.
(6) Engel, M. F. M.; Khemtémourian, L.; Kleijer, C. C.; Meeldijk, H. J. D.; Jacobs, J.; Verkleij, A. J.; de Kruijff, B.; Killian, J. A.; Höppener, J. W. M. *Proc. Natl. Acad. Sci. U.S.A.* **2008**, *105*, 6033.
(7) Cohen, F. E.; Kelly, J. W. *Nature* **2003**, *426*, 905.
(8) Herczenik, E.; Gebbink, M. F. B. G. *FASEB J.* **2008**, *22*, 2115.
(9) Bieschke, J.; Russ, J.; Friedrich, R. P.; Ehrnhoefer, D. E.; Wobst, H.; Neugebauer, K.; Wanker, E. E. *Proc. Natl. Acad. Sci. U.S.A.* **2010**, *107*, 7710.
(10) Daval, M.; Bedrood, S.; Gurlo, T.; Huang, C. J.; Costes, S.; Butler, P. C.; Langen, R. *Amyloid* **2010**, *17*, 118.
(11) Alhamadsheh, M. M.; Connelly, S.; Cho, A.; Reixach, N.; Powers, E. T.; Pan, D. W.; Wilson, I. A.; Kelly, J. W.; Graef, I. A. *Sci. Transl. Med.* **2011**, 3.
(12) Bulic, B.; Pickhardt, M.; Mandelkow, E. M.; Mandelkow, E. *Neuropharmacology* **2010**, *59*, 276.
(13) Gazit, E. *FASEB J.* **2002**, *16*, 77.
(14) Shoval, H.; Lichtenberg, D.; Gazit, E. *Amyloid* **2007**, *14*, 73.
(15) Necula, M.; Kayed, R.; Milton, S.; Glabe, C. G. *J. Biol. Chem.* **2007**, *282*, 10311.
(16) Sellin, D.; Yan, L.-M.; Kapurniotu, A.; Winter, R. *Biophys. Chem.* **2010**, *150*, 73.
(17) Buell, A. K.; Esbjorner, E. K.; Riss, P. J.; White, D. A.; Aigbirhio, F. I.; Toth, G.; Welland, M. E.; Dobson, C. M.; Knowles, T. P. *J. Phys. Chem. Chem. Phys.* **2011**, *13*, 20044.
(18) Porat, Y.; Abramowitz, A.; Gazit, E. *Chem. Biol. Drug Des.* **2006**, *67*, 27.
(19) Hudson, S. A.; Ecroyd, H.; Dehle, F. C.; Musgrave, I. F.; Carver, J. A. *J. Mol. Biol.* **2009**, *392*, 689.
(20) Lopez Del Amo, J. M.; Fink, U.; Dasari, M.; Grelle, G.; Wanker, E. E.; Bieschke, J.; Reif, B. *J. Mol. Biol.* **2012**, *421*, 517.
(21) Armstrong, A. H.; Chen, J.; McKoy, A. F.; Hecht, M. H. *Biochemistry-Us* **2011**, *50*, 4058.
(22) Ehrnhoefer, D. E.; Bieschke, J.; Boeddrich, A.; Herbst, M.; Masino, L.; Lurz, R.; Engemann, S.; Pastore, A.; Wanker, E. E. *Nat. Struct. Mol. Biol.* **2008**, *15*, 558.
(23) Meng, F.; Abedini, A.; Plesner, A.; Verchere, C. B.; Raleigh, D. P. *Biochemistry* **2010**, *49*, 8127.
(24) Norton, R. S.; Chandrashekaran, I. R.; Adda, C. G.; MacRaild, C. A.; Anders, R. F. *Biochemistry* **2010**, *49*, 5899.
(25) Almeida, M. R.; Ferreira, N.; Saraiva, M. J. *FEBS Lett.* **2011**, *585*, 2424.
(26) Lee, S.; Bae, S. Y.; Kim, S.; Hwang, H.; Kim, H. K.; Yoon, H. C.; Kim, J. H.; Kim, T. D. *Biochem. Biophys. Res. Commun.* **2010**, *400*, 531.
(27) Norton, R. S.; Chandrashekaran, I. R.; Adda, C. G.; MacRaild, C. A.; Anders, R. F. *Arch. Biochem. Biophys.* **2011**, *513*, 153.
(28) Saraogi, I.; Hebda, J. A.; Becerril, J.; Estroff, L. A.; Miranker, A. D.; Hamilton, A. D. *Angew. Chem., Int. Ed.* **2010**, *49*, 736.
(29) Meng, F. L.; Raleigh, D. P. *J. Mol. Biol.* **2011**, *406*, 491.
(30) Knight, J. D.; Williamson, J. A.; Miranker, A. D. *Protein Sci.* **2008**, *17*, 1850.
(31) Bazar, E.; Sheynis, T.; Dorosz, J.; Jelinek, R. *ChemBioChem* **2011**, *12*, 761.
(32) Nilsson, M. R. *Methods* **2004**, *34*, 151.
(33) Fu, L.; Ma, G.; Yan, E. C. Y. *J. Am. Chem. Soc.* **2010**, *132*, 5405.
(34) Fu, L.; Liu, J.; Yan, E. C. *J. Am. Chem. Soc.* **2011**, *133*, 8094.
(35) Sovago, M.; Vartiainen, E.; Bonn, M. *J. Phys. Chem. C* **2009**, *113*, 6100.
(36) Nguyen, K. T.; King, J. T.; Chen, Z. *J. Phys. Chem. B* **2010**, *114*, 8291.
(37) Chen, X.; Wang, J.; Sniadecki, J. J.; Even, M. A.; Chen, Z. *Langmuir* **2005**, *21*, 2662.
(38) vandenAkker, C. C.; Engel, M. F. M.; Velikov, K. P.; Bonn, M.; Koenderink, G. H. *J. Am. Chem. Soc.* **2011**, *133*, 18030.
(39) Kapurniotu, A. *Biopol. Pept. Sci.* **2001**, *60*, 438.
(40) Knight, J. D.; Hebda, J. A.; Miranker, A. D. *Biochemistry* **2006**, *45*, 9496.
(41) Lopes, D. H. J.; Meister, A.; Gohlke, A.; Hauser, A.; Blume, A.; Winter, R. *Biophys. J.* **2007**, *93*, 3132.
(42) Mirzabekov, T. A.; Lin, M. C.; Kagan, B. L. *J. Biol. Chem.* **1996**, *271*, 1988.
(43) Kayed, R.; Sokolov, Y.; Edmonds, B.; McIntire, T. M.; Milton, S. C.; Hall, J. E.; Glabe, C. G. *J. Biol. Chem.* **2004**, *279*, 46363.
(44) Butterfield, S. M.; Lashuel, H. A. *Angew. Chem., Int. Ed.* **2010**, *49*, 5628.
(45) Padrick, S. B.; Miranker, A. D. *Biochemistry* **2002**, *41*, 4694.
(46) Engel, M. F. M.; Yigittop, H.; Elgersma, R. C.; Rijkers, D. T. S.; Liskamp, R. M. J.; de Kruijff, B.; Höppener, J. W. M.; Killian, J. A. *J. Mol. Biol.* **2006**, *356*, 783.
(47) Jayasinghe, S. A.; Langen, R. *Biochim. Biophys. Acta* **2007**, *1768*, 2002.
(48) Murphy, R. M. *Biochim. Biophys. Acta* **2007**, *1768*, 1923.
(49) Knight, J. D.; Miranker, A. D. *J. Mol. Biol.* **2004**, *341*, 1175.
(50) Koo, B. W.; Hebda, J. A.; Miranker, A. D. *Protein Sci.* **2008**, *21*, 147.
(51) Demel, R. A.; Geurts van Kessel, W. S.; Zwaal, R. F.; Roelofsen, B.; van Deenen, L. L. *Biochim. Biophys. Acta* **1975**, *406*, 97.
(52) Smits, M.; Sovago, M.; Wurpel, G. W. H.; Kim, D.; Muller, M.; Bonn, M. *J. Phys. Chem. C* **2007**, *111*, 8878.
(53) LeVine, H., III *Methods Enzymol.* **1999**, *309*, 274.
(54) Ege, C.; Lee, K. Y. C. *Biophys. J.* **2004**, *87*, 1732.
(55) Canale, C.; Torrassa, S.; Rispoli, P.; Relini, A.; Rolandi, R.; Bucciantini, M.; Stefani, M.; Gliozzi, A. *Biophys. J.* **2006**, *91*, 4575.
(56) Gopal, A.; Lee, K. Y. *J Phys. Chem.B* **2006**, *110*, 22079.

(57) Wang, J.; Even, M. A.; Chen, X. Y.; Schmaier, A. H.; Waite, J. H.; Chen, Z. *J. Am. Chem. Soc.* **2003**, *125*, 9914.
(58) Castner, D. G.; Weidner, T.; Apte, J. S.; Gamble, L. J. *Langmuir* **2010**, *26*, 3433.
(59) Arrondo, J. L. R.; Muga, A.; Castresana, J.; Goni, F. M. *Prog. Biophys. Mol. Biol.* **1993**, *59*, 23.
(60) Nanga, R. P. R.; Brender, J. R.; Vivekanandan, S.; Ramamoorthy, A. *Biochim. Biophys. Acta* **2011**, *1808*, 2337.
(61) Huh, N. W.; Porter, N. A.; McIntosh, T. J.; Simon, S. A. *Biophys. J.* **1996**, *71*, 3261.
(62) Nakayama, T.; Kajiya, K.; Kumazawa, S. *Biosci. Biotechnol. Biochem.* **2002**, *66*, 2330.